

N. G. Dagalakis

J. S. Albus

B.-L. Wang

J. Unger

J. D. Lee

Robot Systems Division,
National Bureau of Standards,
Gaithersburg, MD 20899

Stiffness Study of a Parallel Link Robot Crane for Shipbuilding Applications

This describes the first phase of an effort to develop a robot crane for shipbuilding applications. The focus of this phase is on the study of the stiffness characteristics of this robot as a function of its geometry payload and height. A brief description of the design of the main part of the robot crane consisting of a six-wire parallel link manipulator is given. The stiffness of the manipulator to side loads and moments was studied. The nonlinear and linearized mathematical model of the manipulator stiffness matrix is derived. Stiffness measurement tests were conducted using a small size laboratory model. The results of these tests for various external loads, heights, and payloads are given. Computer simulation and theoretical results are also discussed.

Introduction

The last ten years have seen a tremendous growth in the use of robots in the manufacturing industry with more than 20,000 units installed in the U.S., most of them in the automotive or automotive-related industries (U.S. Department of Commerce, 1987). Amidst this astounding technological development there are very few applications of robots in the heavy construction industry and large-scale assembly, like shipbuilding. The reasons for that delay are probably due to the fact that shipbuilding is a made-to-order industry, requiring great precision in the construction of components and blocks, requiring an enormous number of structural members and machines most of which are heavy and bulky. Shipbuilding construction, being labor intensive, is becoming more expensive every year, while robotic automation is becoming less expensive and more capable every year. Perhaps the time has come for the two technologies to intersect and to help each other enhance their cost competitiveness and productivity.

In Japan, the Japanese Shipbuilding Society started a 5-yr research and development plan of "Modernization of Production Technology in Japan" on 1982 (Kubo, 1987). The program is sponsored by a consortium of seven major Japanese shipbuilders, and funded by the Japan Foundation for Shipbuilding Advancement. As a result of this effort, prototypes of large size gantry-type robots for welding, surface preparation and painting of ship structures have been built by Ishikawajima-Harima Heavy Industries Co. and are now being tested by Sumitomo Heavy Industries, Ltd.

One significant part of shipbuilding activity involves handling, lifting, positioning and assembling of large and small ship components and machinery. These operations are not

only labor intensive, but dangerous and tiring too. For example, end load outfitting involves transfer of loads from a crane to hand rigging equipment. Lateral translation of the load usually involves additional transfers or trolleys running on rails temporarily attached to ship structure. Installation and operation of hand rigging equipment is heavy labor-intensive work, and each load transfer is a potentially very dangerous evolution. Many ship system components must be landed on foundation or inserted with precise lateral position orientation and declivity. Additional rigging, tag lines and contact forces applied by rigging personnel are used to make these landings. Hands and feet in way of the lift are in danger of being crushed by slack loads suddenly seating. Often final alignment must be made with jack screws, wedges and gibs.

Currently, ordinary shipyard cranes are stable only in the vertical direction. The load is free to rotate in all directions and sway in the horizontal plane under the slightest side pressure, like a pendulum does. Under these conditions it would be very difficult for the crane to support any robotic operations due to the excessive compliance of its end effector. Automatic crane antisway control devices have been proposed and tested by several people (Kogure, et al., 1978; Carbon, 1976; Gercke, U.S. Patent No. 2,916,162). Although these devices tend to suppress the pendulum motions in the horizontal directions, they fail to suppress any pitch, roll or yaw rotations of the load. Other systems have been developed which try to solve the sway problem by employing several wires and winches (Noly, U.S. Patent No. 4,350,254). These systems add considerable complexity and cost to the load-handling system and have not found practical application thus far.

Conventionally designed robots could be used as shipyard cranes, but they would probably be impractical for handling heavy loads. Considering the low payload to manipulator arm weight ratio of these robots, they would have to be constructed of gigantic dimensions, occupy a large area of the shipyard ground, and consume large amounts of power.

Contributed by the OMAE Division and presented at the Seventh International Conference on Offshore Mechanics and Arctic Engineering, Houston, Texas, February 7-12, 1988, of THE AMERICAN SOCIETY OF MECHANICAL ENGINEERS. Manuscript received by the OMAE Division, 1987; revised manuscript received September 12, 1988.

In this paper we propose a new crane design, which despite its simplicity, results in a very stiff load platform which can be used as a robot base or end effector for heavy loads. A nonlinear and a linearized model of the crane stiffness to external loads are derived. A small size model of the proposed crane was constructed and its stiffness to external side loads was measured.

The Proposed Robot Crane Design

Considering the requirements for a robot crane, which should provide superior stiffness to load roll and sway, has a large work volume without occupying any significant floor space and has a reasonable size, the mechanism concept shown in Fig. 1 is proposed. It consists of an equilateral triangular platform which will be suspended by six wireropes, two at each vertex of the triangle, from an overhead carriage. The carriage can be attached to either an overhead (see Fig. 2) or a boom crane depending on the application. The carriage includes a single winch onto which all six wireropes attach and rope guides which guide the six wireropes away from the winch in three pairs equidistantly spaced. If desired, it is possible to adjust the lengths of the individual wireropes with actuators which are mounted between the carriage and the guides. Adjusting the lengths of the wireropes will result in a change of the position and orientation of the suspended platform and the rope tensions (Albus, 1987).

The suspended platform behaves as if the six wireropes were an extensible single solid beam with a spring constant dependent on the weight of the load and the height of the crane for a given crane geometry and wireropes type and size. This is a significant improvement in stiffness over a conventional crane and it enables the load to be accurately positioned and provides a stable platform which can be used to exert torques and side forces on objects being positioned. The suspended platform can be used as a stabilized base for the direct mounting of conventional manipulator arms or it can be used for the support of special substructures for specific crane applications. For example, to extend the reach inside closed spaces a subplatform load handling mechanism can be used which will enable shipyards to accomplish end load outfitting of ship modules and precision handling of ship system components with improved productivity and personnel safety. To extend the reach inside closed spaces, a folding substructure mechanism can be used in order to pass through narrow openings and then unfold to cover the desired inner space volume.

The suspension mechanism of the proposed robot crane platform shown in Fig. 1 imitates the behavior of a parallel

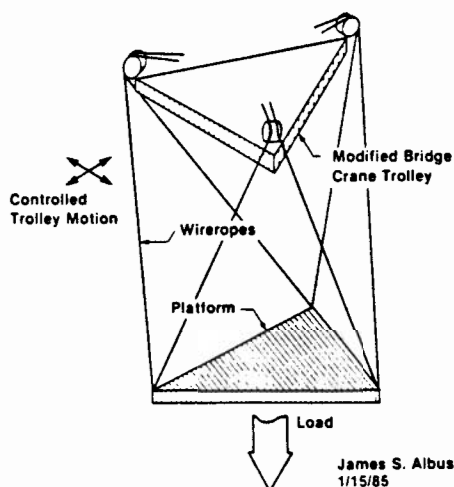


Fig. 1 Mechanism concept

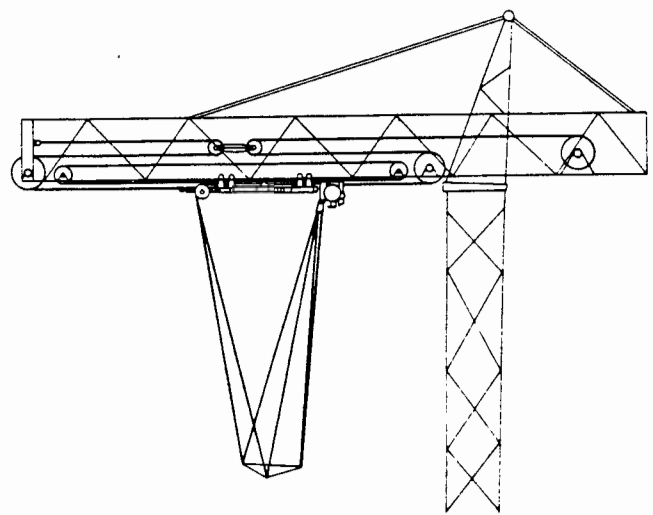


Fig. 2 Overhead robot crane

link manipulator arm. The arm mechanism is called that because the links are positioned side by side, "approximately" parallel to each other and each link serves a role "approximately" equal to that of its neighbor. This is different than the design of the more common serial link manipulators built of a chain of links connected end to end in a serial manner. Parallel link manipulators are in general known for the simplicity of their mechanical design, and their high strength and stiffness-to-weight ratios, because their actuators bear no moment loads but act in simple tension or compression. They are also known for their high force and moment capacity, since their actuators act all in parallel. Such manipulators with solid adjustable length beams in the place of the wireropes were first used for the design of tyre test machines (Gough, et al., 1957, 1962); later they were used for the design of flight simulators (Stewart, 1965). With the increasing interest in robotic arm manipulators, studies have been conducted for its use as a mechanical wrist (Bennett, 1968), a compliant device (McCallion et al., 1979), a force/moment or position sensor (Koliskor, 1982), a robot arm (Fichter et al., 1980, 1984, 1987; Powell, 1982; Landsberger, et al., 1985; Sheridan, 1986; Konstantinov et al., 1985), and an industrial manipulator for assembly (Gadfly, 1983) and for grinding (Multicraft, 1987).

The design discussed in this paper is taking advantage of the suspended crane load to maintain the wireropes extended, and thus form six flexible wires which, with their elastic deformation, oppose any displacement of the payload. The stiffness created by this elastic deformation is superimposed onto the pendulum-effect-created-stiffness of ordinary cranes. Individual rope length control of the position and orientation of the platform is possible, but it is probably difficult for the length of the wires considered here, energy-consuming for the payloads considered, and not necessary if the responsibility for the manipulation control is placed on the end-effector device which will be suspended from the platform.

Nonlinear Model Stiffness Study

This section describes the development of a computer model of the robot crane stiffness based on the nonlinear equations of the quasi-static motion of the lower platform. For a given external load (force and/or moment), applied to the center of gravity of the lower platform, the computer program solves the force and moment balance equations of the platform and wireropes support system to determine the corresponding three-dimensional space displacement. The

relationship between the six Cartesian coordinate frame components of the load and the components of displacement expresses the stiffness of the crane structure.

The basic structure of the robot crane, which consists of the wirerope support system, is shown in Fig. 3 for the resting steady-state position. The overhead carriage and the suspended platform are represented by two equilateral triangles. In this position both triangles are assumed to be horizontal with their centers of gravity lying on the vertical axis z . The overhead triangle is assumed to be fixed in space and has three vertices located at

$$\begin{aligned} A: & (-b, -b\sqrt{3}/3, -h) \\ B: & (b, -b\sqrt{3}/3, -h) \\ C: & (0, 2b\sqrt{3}/3, -h) \end{aligned} \quad (1)$$

with respect to a fixed Cartesian coordinate frame (x, y, z) , based on the lower triangle, when it is positioned at its steady-state resting stage, and centered at its center of gravity, (see Fig. 3). Where $2b$ is the length of the side of the overhead triangle and $2a$ is the length of the side of the lower triangle. The height h is the vertical distance between the two triangles.

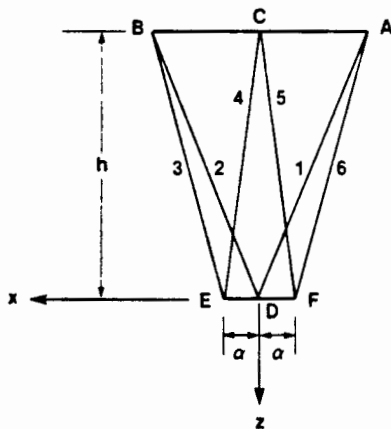
The lower triangle, before it is displaced, has three vertices located at

$$\begin{aligned} D: & (0, -2a\sqrt{3}/3, 0) \\ E: & (a, a\sqrt{3}/3, 0) \\ F: & (-a, a\sqrt{3}/3, 0) \end{aligned} \quad (2)$$

with respect to the same coordinate frame.

The two triangles are connected by the six elastic wires, $\{AD, BD, BE, CE, CF, AF\}$. Before the lower triangle is displaced, all six wires have the resting steady-state length, which is

$$l_0 = \sqrt{h^2 + 4(b^2 + a^2 - ab)/3} \quad (3)$$



Front View

Top View

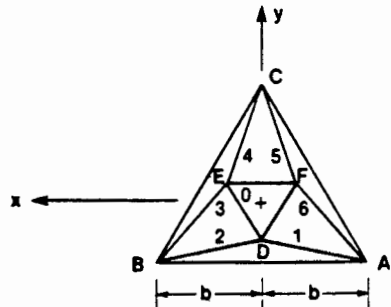


Fig. 3 Robot crane wirerope support structure

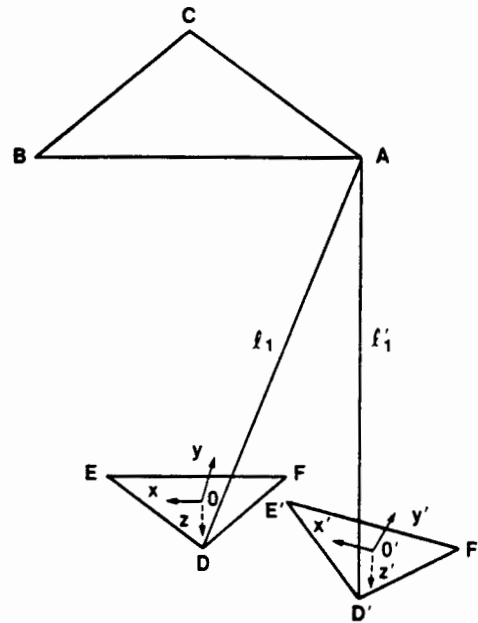


Fig. 4 Displaced lower platform and no. 1 wire rope

Let the lower triangle undergo a rigid body motion (see Fig. 4) characterized by three displacements, u_x, u_y, u_z , and three successive rotations, performed in the following sequence: first, rotation by an angle ϕ about z^* -axis, then θ about x^* -axis, and then ψ about y^* -axis. Here x^* -axis, y^* -axis, z^* -axis, called the body axes, are the three axes embedded in the lower triangle, which coincide with the x -axis, y -axis, z -axis, before any motion takes place. If (x, y, z) and (x', y', z') are the coordinates of any point on the lower triangle before and after the motion, respectively, then the coordinate transformation between the two can be written as

$$\begin{bmatrix} x' \\ y' \\ z' \end{bmatrix} = \underline{Q} \begin{bmatrix} x \\ y \\ z \end{bmatrix} + \begin{bmatrix} u_x \\ u_y \\ u_z \end{bmatrix} \quad (4)$$

where the rotational transformation matrix \underline{Q} can be expressed in terms of the previously mentioned angles of rotation as (Goldstein, 1950)

$$\underline{Q} = \begin{bmatrix} \cos \psi \cos \phi - \sin \psi \sin \theta \sin \phi & \cos \psi \sin \phi + \sin \psi \sin \theta \cos \phi & -\sin \psi \cos \theta \\ -\cos \theta \sin \phi & \sin \psi \cos \phi + \cos \psi \sin \theta \sin \phi & \sin \psi \sin \phi - \cos \psi \sin \theta \cos \phi \\ \sin \theta & \cos \psi \cos \theta & \cos \psi \cos \theta \end{bmatrix} \quad (5)$$

Applying the transformation equations (4) and (5) on the coordinates of the vertices D, E, F , of the lower triangle gives the coordinates of the same vertices at the new locations D', E', F' after the end of the rigid body motion

$$\begin{aligned} D': & (-2aQ_{12}\sqrt{3}/3 + u_x, -2aQ_{22}\sqrt{3}/3 \\ & + u_y, -2aQ_{32}\sqrt{3}/3 + u_z), \\ E': & (aQ_{11} + aQ_{12}\sqrt{3}/3 + u_x, aQ_{21} \\ & + aQ_{22}\sqrt{3}/3 + u_y, aQ_{31} + aQ_{32}\sqrt{3}/3 + u_z), \\ F': & (-aQ_{11} + aQ_{12}\sqrt{3}/3 + u_x, -aQ_{21} \\ & + aQ_{22}\sqrt{3}/3 + u_y, -aQ_{31} + aQ_{32}\sqrt{3}/3 + u_z) \end{aligned} \quad (6)$$

where Q_{ij} is the i th row, j th column element of matrix \underline{Q} given by equation (5).

The vectors l_n' ($n = 1, \dots, 6$) defining the new position of the wires can be found from (1) and (6), and are expressed as

$$l_1' = \Delta - D' = (-b + 2aQ_{12}\sqrt{3}/3 - u_x, -b\sqrt{3}/3 + 2aQ_{22}\sqrt{3}/3 - u_y, -h + 2aQ_{32}\sqrt{3}/3 - u_z) \quad (7)$$

$$l_2' = B - D' = (b + 2aQ_{12}\sqrt{3}/3 - u_x, -b\sqrt{3}/3 + 2aQ_{22}\sqrt{3}/3 - u_y, -h + 2aQ_{32}\sqrt{3}/3 - u_z) \quad (8)$$

$$l_3' = B - E' = (b - aQ_{11} - aQ_{12}\sqrt{3}/3 - u_x, -b\sqrt{3}/3 - aQ_{21} - aQ_{22}\sqrt{3}/3 - u_y, -h - aQ_{31} - aQ_{32}\sqrt{3}/3 - u_z) \quad (9)$$

$$l_4' = C - E' = (-aQ_{11} - aQ_{12}\sqrt{3}/3 - u_x, 2b\sqrt{3}/3 - aQ_{21} - aQ_{22}\sqrt{3}/3 - u_y, -h - aQ_{31} - aQ_{32}\sqrt{3}/3 - u_z) \quad (10)$$

$$l_5' = C - F' = (aQ_{11} - aQ_{12}\sqrt{3}/3 - u_x, 2b\sqrt{3}/3 + aQ_{21} - aQ_{22}\sqrt{3}/3 - u_y, -h + aQ_{31} - aQ_{32}\sqrt{3}/3 - u_z) \quad (11)$$

$$l_6' = \Delta - F' = (-b + aQ_{11} - aQ_{12}\sqrt{3}/3 - u_x, -b\sqrt{3}/3 + aQ_{21} - aQ_{22}\sqrt{3}/3 - u_y, -h + aQ_{31} - aQ_{32}\sqrt{3}/3 - u_z) \quad (12)$$

After the rigid body motion, the length of the wirerope will in general be different. Let the length of the n th vector l_n' be denoted by l_n' , which can be determined from

$$l_n' = \sqrt{l_{n1}'^2 + l_{n2}'^2 + l_{n3}'^2} \quad (13)$$

where l_{n1}' , l_{n2}' , l_{n3}' are the lower platform (x, y, z) frame projections of wirerope vector l_n' . The length of the n th wirerope, if it is in tension, is equal to l_n' .

The force acting on the lower platform triangle, due to the change in tension of the n th wirerope, as a result of the rigid body motion is given by

$$f_n = \begin{cases} k(l_n' - l_0)l_n'/l_n', & l_n' \geq l_0 \\ 0, & l_n' < l_0 \end{cases} \quad (14)$$

where k is the stiffness of the wirerope. It is assumed here that the wirerope cannot support compressive forces; therefore, if l_n' becomes less than l_0 , the force on the n th wirerope becomes zero.

The balance of forces acting on the lower platform requires that

$$f + \sum_{n=1}^6 f_n = 0 \quad (15)$$

where f is the external force applied at the center of gravity of the platform.

The balance of moments acting on the lower platform requires that

$$m + QD \times (f_1 + f_2) + QE \times (f_3 + f_4) + QF \times (f_5 + f_6) = 0 \quad (16)$$

where m is the external moment applied upon the lower platform.

Notice that due to the complexity of the six wirerope system kinematics, equations (15), (16) are highly nonlinear. If $u_x, u_y, u_z, \phi, \theta, \psi$, are given then it is straightforward to solve for the force and moment f and m needed to maintain the balance of the lower platform. On the other hand, for a given external force f and moment m , equations (15), (16)

have to be solved iteratively to determine $u_x, u_y, u_z, \phi, \theta, \psi$, which specify the position and orientation of the lower platform.

A computer program was developed to iteratively solve equations (15), (16) and to determine the rigid body movement of the proposed lower robot crane platform as a function of the applied external load. The numerical results generated by the computer program are compared with experimental test data. The results of that comparison will be discussed in a later section.

Linearized Model Stiffness Study

If the rigid body motion displacements of the lower platform are small, it is possible to linearize equations (15) and (16) in terms of those displacements about the resting steady-state position for a total suspended weight of the lower platform, substructure, payload, etc., of W . The linearization results in a significant simplification of the nonlinear force and moment balance equations (15), (16), which can then be solved to derive an analytical expression between the external lower platform load and the resulting displacements

$$P = K\delta u \quad (17)$$

where the stiffness matrix K is given by

$$K = \begin{bmatrix} K_1 & 0 & 0 & 0 & -K_2 & 0 \\ 0 & K_1 & 0 & K_2 & 0 & 0 \\ 0 & 0 & K_3 & 0 & 0 & 0 \\ 0 & K_2 & 0 & K_4 & 0 & 0 \\ -K_2 & 0 & 0 & 0 & K_4 & 0 \\ 0 & 0 & 0 & 0 & 0 & K_5 \end{bmatrix} \quad (18)$$

$P = [f, f, f, m, m, m]^T$ is the vector of the external load of force f and moment m , $\delta u = [\delta u, \delta u, \delta u, \delta\theta, \delta\psi, \delta\phi]^T$ is the vector of the resulting displacements, and

$$K_1 = 4k(a^2 + b^2 - ab) \frac{l_0}{l_w^3} + \frac{W}{h_w}$$

$$K_2 = 2ka(2a - b)h_w \frac{l_0}{l_w^3}$$

$$K_3 = 6kh_w^2 \frac{l_0}{l_w^3} + \frac{W}{h_w}$$

$$K_4 = 4ka^2h_w^2 \frac{l_0}{l_w^3} + ab \frac{W}{3h_w}$$

$$K_5 = 8ka^2b^2 \frac{l_0}{l_w^3} + ab \frac{2W}{3h_w}$$

$$l_w = \sqrt{h_w^2 + 4(b^2 + a^2 - ab)/3} \quad h_w = \frac{W}{6k(l_w - l_0)}$$

l_w and h_w are the resting steady-state position wirerope length and the height of the lower platform from the overhead carriage, respectively, after the application of the weight W with no external load. l_0 is the resting steady-state position wirerope length for zero weight and no external load given by equation (3). k is the wirerope stiffness assumed to be the same for all six of them.

The elements of the linearized system stiffness matrix are relatively simple expressions of the robot crane dimensions, the wirerope stiffness, and the suspended total weight W . K_1, K_2, K_3, K_4, K_5 , consist of two terms, and, as the suspended weight is reduced to zero, the first term is reduced to a function of the geometry and the wirerope stiffness while the second term is reduced to zero. However, the reduction of the first term is much smaller than that of the second term.

It is shown in Appendix I that the first term of K_j , ($j = 1$ to 5), is that component of stiffness which is due to the elastic deformation of the wirerope, acting as linear springs, when there is no suspended weight ($W = 0$). It is shown in Appendix II that the second term of K_j , is due to the pendulum-induced stiffness by the suspended weight W .

Experimental Setup and Test Results

A small model of the proposed robot crane suspension mechanism was constructed in order to test the validity of the mathematical stiffness model. The model consisted of two aluminum triangular plates, like the ones shown in Fig. 1, of equal side length $a = b = 114.3$ mm (4.5 in.). The lower platform was suspended by six steel wires of 1.08-mm (0.042-in.) diameter. Measuring the speed of sound propagation inside the wires it was determined that the modulus of elasticity of the material was $E = 206,831 \times 10^6$ N/m² (30×10^6 lbf/in²). The wire stiffness for each test was determined from $k = AE/l_0$, where A is the wire cross-sectional area. The height h and the suspended weight W varied depending on the test conditions. During testing external loads (force or moment) of various amplitudes and orientations were applied through a multiaxis load-cell. The resulting displacement in the direction of load application was measured with a Linear Voltage Differential Transducer (LVDT). The test results were plotted and compared with the ones predicted by the mathematical model.

The model crane tests attempted to simulate the type of external loads which are anticipated to dominate the loading of the real robot crane during operation. Single coordinate axis direction external loads were applied during each test. One series of tests involved the application of a single external force on the lower platform in the horizontal direction, a second series of tests involved the application of a force in the vertical direction along the axis of symmetry, and a third series of tests involved the application of a pure moment along the vertical direction axis of symmetry.

Single External Force in the Horizontal Direction. During this series of tests a single horizontal force was applied on the lower platform in the y -axis direction, as is shown in Fig. 3. The amplitude of the force, the length of the wires l_0 , and the total supported weight W were varied. Figure 5 shows the external force f_j versus the displacement δu_j plot from the experimental test data for a certain wire length l_0 and total suspended weight W combination. As can be seen from that figure for the range of external forces used in this test the relationship between force and displacement is close to linear.

To check the accuracy of the theoretical model to predict the experimental data, the external force f_j versus the displacement δu_j relationship from the nonlinear mathematical model was plotted on the same figure. This plot is represented by the solid line on Fig. 5. The same was done for the linearized mathematical model and it was found that the two lines are indistinguishable on that figure. As can be seen from those plots, the theoretical models predict the crane suspension mechanism stiffness accurately.

Solving equation (17) for an external load vector $P_1 = [0, f_j, 0, 0, 0]^T$ gives

$$f_j = K_j \delta u_j,$$

where

$$K_j = \left(K_1 - \frac{K_2^2}{K_4} \right) \quad (19)$$

substituting for K_1 , K_2 , K_4 , gives a complex expression of K_j in terms of k , a , l_0 , and W .

To get a better physical understanding of the source of this stiffness, the external force f_j versus the displacement δu_j from

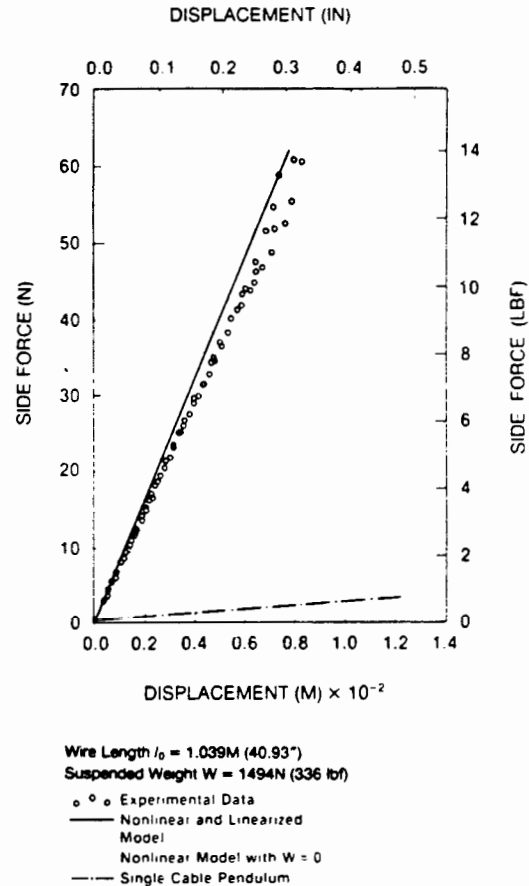


Fig. 5 Experimental testing and computer simulation results

the mathematical models was plotted for the case when there is no suspended weight ($W = 0$), shown by the dotted line of Fig. 5. This is equivalent to considering only the first term of K_j , ($j = 1$ to 5), representing that component of stiffness which is due to the elastic deformation of the six wires. The remaining part of the total stiffness, up to the solid line in the figure, corresponds to the pendulum-induced stiffness by the suspended weight W .

For comparison purposes, the external force f_j versus the displacement δu_j , of a single wire pendulum mathematical model with $1/6$ the suspended weight W was also plotted, shown by the dashed line of Fig. 5. It is obvious that a crane constructed that way would have a fraction of the stiffness of the proposed robot crane to horizontal external loads.

Figure 6 shows the results of a similar test for a lighter suspended weight W . As can be seen again the mathematical models predict the stiffness with good accuracy. For lighter weights the pendulum-induced component of the stiffness decreases.

Figures 7 and 8 show the external force f_j versus the displacement δu_j plots for the same suspended weights W but longer wire length l_0 . Comparing these figures with Figs. 5 and 6 shows a significant decrease of stiffness as a result of the increase in the wire length. This time both components of stiffness are affected. The Fig. 9 plot reveals an interesting phenomenon caused by the combination of low suspended weight W and long wire length l_0 . For low external side force values f_j there appears to exist a linear relationship between f_j and δu_j . As the value of the side force increases though it results in larger and larger displacements of the lower platform resulting in a nonlinear relationship between f_j and δu_j . Closer examination of the model revealed that this was caused by the buckling of the suspension wires as they reached the zero tension level. The phenomenon was simulated by the com-

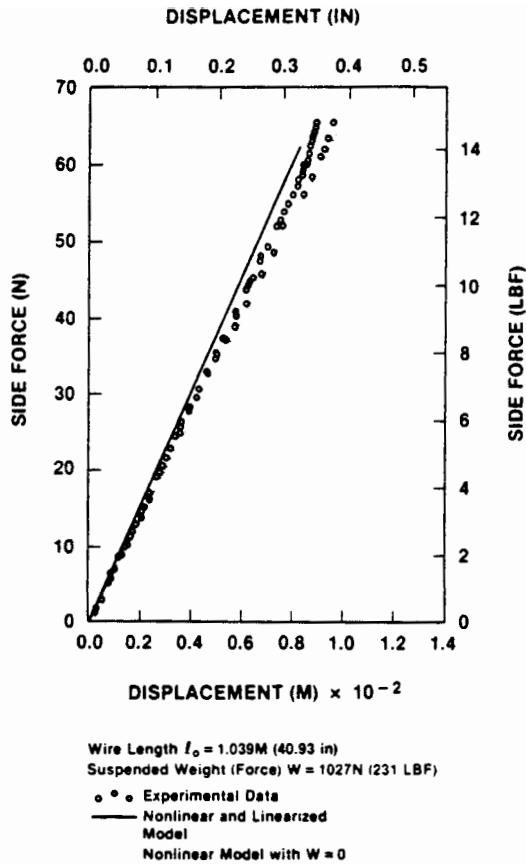


Fig. 6 Experimental testing and computer simulation results

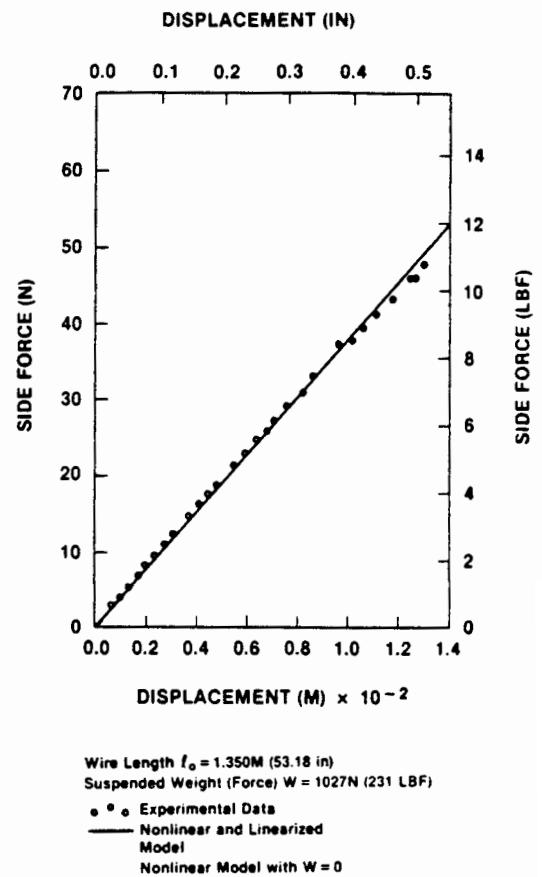


Fig. 8 Experimental testing and computer simulation results

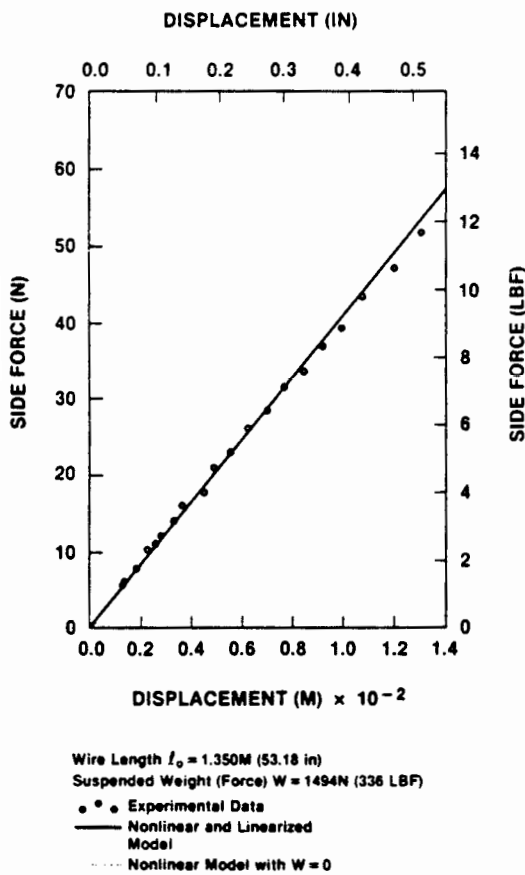


Fig. 7 Experimental testing and computer simulation results

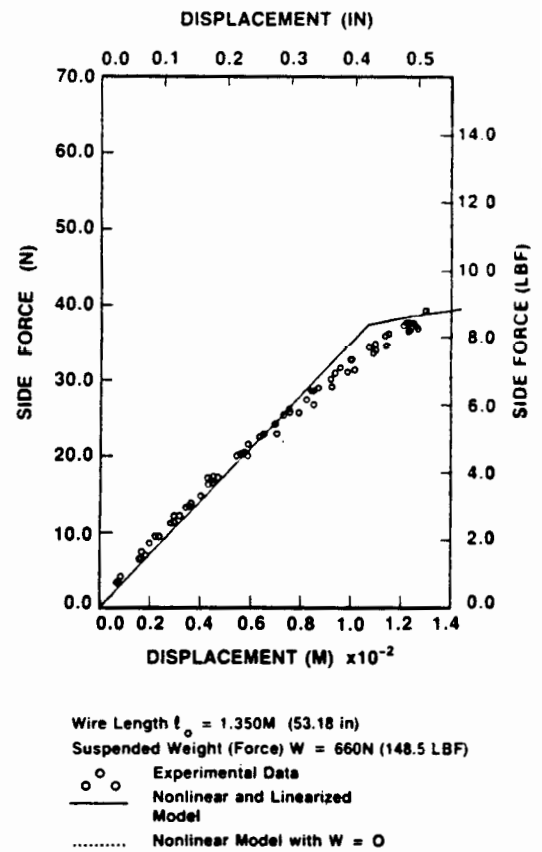


Fig. 9 Experimental testing and computer simulation results

puter model by setting the wire tension to zero as soon as it reached negative values. The computer simulation plot is shown on the same figure.

Figure 10 shows how the stiffness, to an external force f_1 , varies with the suspended weight and wire length. For this figure the stiffness was calculated from the computer model assuming small external forces and displacements. As can be seen from this figure, the stiffness can be assumed to be a linear function of the suspended weight W , for the model dimensions considered here. This can be verified from equation (19) after substituting for the numerical values. The coefficients of all the nonlinear W terms are very small and can be ignored.

Single External Moment in the Vertical Direction. During this series of tests a single moment was applied on the lower platform in the z-axis direction, as is shown in Fig. 3. The amplitude of the moment, and the total supported weight W' were varied. From equation (18) it can be seen that the expected stiffness to that type of load is K_z .

Figures 11 and 12 show the external moment M_z versus the angular displacement $\delta\phi$ plot from the experimental test and computer model data for a certain wire length l_0 and two different suspended weights W' . As can be seen from those figures for the range of external moments used in this test, the relationship between moment and angular displacement is very close to linear. There is a small drop in the pendulum component of stiffness due to the decrease of the suspended weight. In this case it appears that the stiffness is dominated by the component of stiffness due to the elastic deformation of the wires.

Figure 13 shows how the stiffness, to an external moment M_z , varies with the suspended weight and wire length. For this figure the stiffness was calculated from the computer model assuming small external moments and displacements. As can be seen, from this figure, the stiffness can be assumed

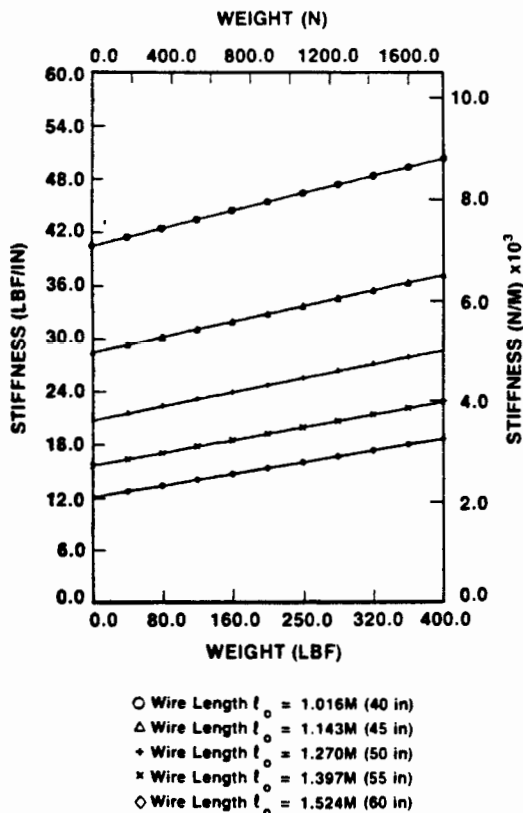


Fig. 10 Computer model results

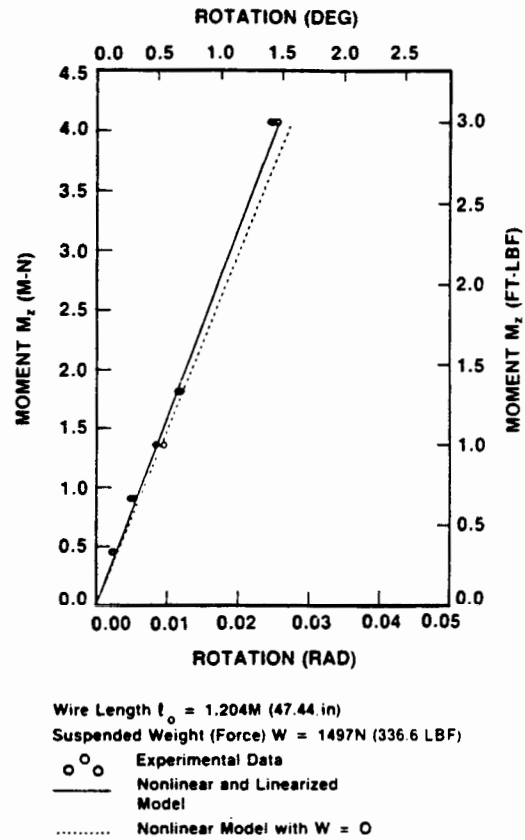


Fig. 11 Experimental testing and computer simulation results

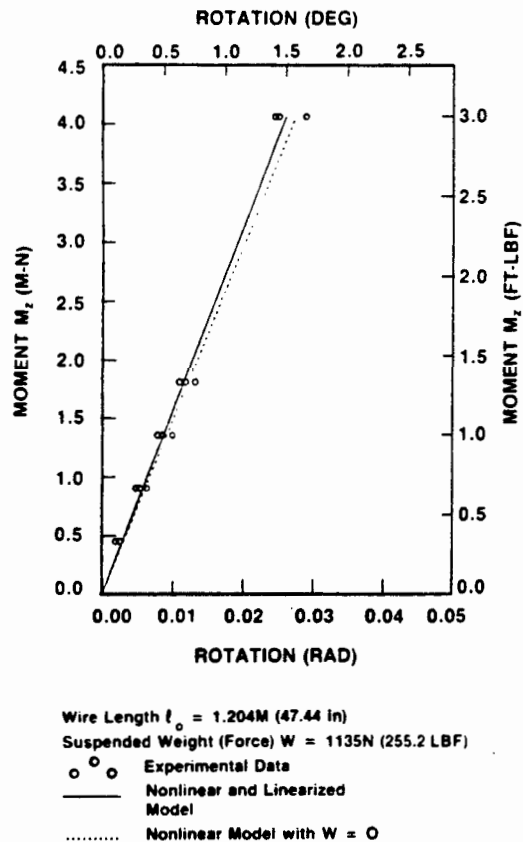


Fig. 12 Experimental testing and computer simulation results

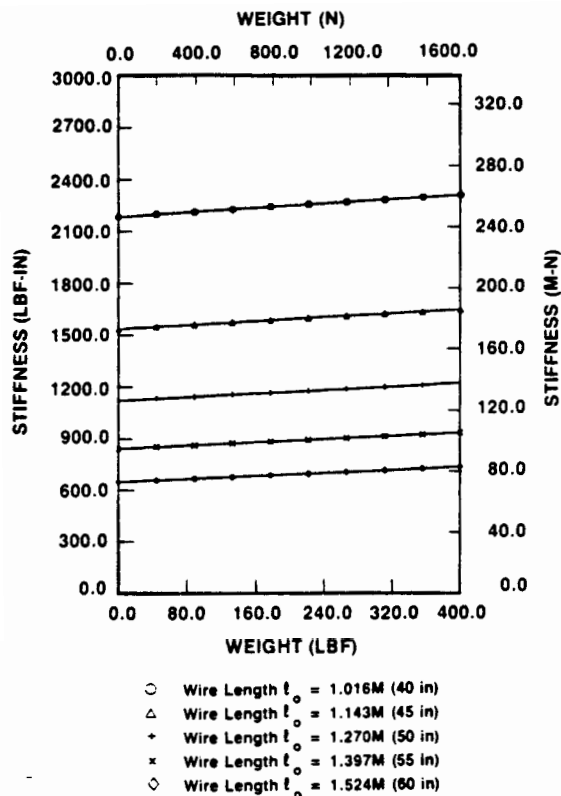


Fig. 13 Computer model results

to be a linear function of the suspended weight W , for the model dimensions considered here.

Single External Force in the Vertical Direction. During this series of tests a single force was applied on the lower platform in the z -axis direction, as is shown in Fig. 3. The amplitude of the force, and the total supported weight W were varied. From equation (18) it can be seen that the expected stiffness to that type of load is K_3 . The experimentally measured stiffness came close to that value.

Conclusions

The linearized mathematical model of the proposed robot crane suspension mechanism of equation (18) seems to provide an adequate prediction of the lower platform external load to displacement relationship, at least for the experimentally tested cases and for small displacements.

For small displacements the overall stiffness seems to consist of the superposition of two terms; the first is due to the elastic deformation of the suspension wires, acting as linear springs, and the second is due to the pendulum stiffness induced by the suspended weight.

A decrease in the suspended weight magnitude causes a decrease of the pendulum component of stiffness. An increase in the wire length causes a significant decrease in overall stiffness. In this case both components of stiffness are affected.

The stiffness can be assumed to be a linear function of the suspended weight for the chosen model dimensions and range of weights.

The stiffness of the proposed robot crane mechanism is significantly higher than that of a conventional single-wire crane.

Of course, these conclusions apply only for the selected robot crane design of the two equilateral triangles and six wireropes shown in Fig. 1. The analysis technique used though is general and independent of the selected design.

Acknowledgment

The assistance of Dr. Donald Myers and Mr. Mitchell Tarica for the construction and the first testing of the model crane was greatly appreciated. We would like to thank Mr. Stephen Lamkin for preparing the plots of some of the figures in this paper.

This work was partially supported by the Defense Advanced Research Project Agency (DARPA) under ARPA Order no. 6380.

References

- Albus, J. S., 1987, internal report.
 Asada, H., and Slotine, J.-J. E., 1986, *Robot Analysis and Control*, John Wiley and Sons.
 Bennett, W. M., 1968, "Mechanical Wrist for a Robot Arm," Mechanical Engineering Department: Massachusetts Institute of Technology, B.S. thesis.
 Carbon, L., 1976, "Automation of Grab Cranes," *Siemens Review*, Vol. 43, No. 2, Feb., pp. 80-85.
 Fichter, E. F., and McDowell, E. D., 1980, "A Novel Design for a Robot Arm," *Proceedings, International Computer Technical Conference*, San Francisco, Calif., Aug., pp. 250-256.
 Fichter, E. F., 1984, "Kinematics of a Parallel Connection Manipulator," ASME Paper 84-DET-45 delivered at the Design Engineering Technical Conference, Cambridge, Mass., Oct.
 Fichter, E. F., 1987, "A Stewart Platform Based Manipulator: General Theory and Practical Construction," *The Kinematics of Robot Manipulators*, MIT Press, pp. 165-190.
 1983, "Gadfly—The Answer to Electronic Component Assembly," *Assembly Automation*, Feb., pp. 20-22.
 Goldstein, H., 1950, *Classical Mechanics*, Addison-Wesley Publishing, Co., Reading, Mass.
 Gough, V. E., 1956-1957, "Contribution to Discussion of Papers on Research in Auto Stability and Control and in True Performance by Cornell Staff," *Proceedings, Auto Division Institute of Mechanical Engineers*, pp. 392-403.
 Gough, V. E., and Whitehall, S. G., 1962, "Universal Tyre Test Machine," *Proceedings, 9th International Automobile Technical Congress*, pp. 117-135.
 Kogure, H., and Tojo, M., 1978, "Recent Developments in Crane Control," *Hitachi Review*, Vol. 27, No. 6, pp. 315-320.
 Koliskor, A. S., 1982, "Development and Investigation of Industrial Robots Based on Specification by l-Coordinates," *Soviet Engineering Research*, Vol. 2, No. 12, pp. 75-78.
 Konstantinov, M. S., Sotirov, Z. M., Zamanov, V. B., and Nenchev, D. N., 1985, "Force Feedback Control of Parallel Topology Manipulating Systems," *Proceedings, 15th International Symposium on Industrial Robots*, Tokyo, Japan, Sept., pp. 181-188.
 Kubo, M., 1987, "Robots and Computers to Automate Japanese Shipbuilding," Keynote Address II, 6th International Symposium on Offshore Mechanics and Arctic Engineering, Houston, Tex., Mar.
 Landsberger, S. E., and Sheridan, T. B., 1985, "A New Design for Parallel Link Manipulators," *Proceedings, Systems Man and Cybernetics Conference*, Tuscon, Ariz., Nov., pp. 812-814.
 McCallion, H., Johnson, G. R., and Pham, D. T., 1979, "A Compliant Device for Inserting a Peg in a Hole," *The Industrial Robot*, June, pp. 81-87.
 McCallion, H., and Truong, P. D., 1979, "The Analysis of a Six Degree-of-Freedom Work Station for Mechanised Assembly," *Proceedings, 5th World Congress on Theory of Machines and Mechanisms*, Montreal, Canada, July, pp. 611-616.
 Multicraft A/S, Oslo, Norway.
 Powell, I. L., 1982, "The Kinematic Analysis and Simulation of the Parallel Topology Manipulator," *The Marconi Review*, Vol. XLV, No. 226, 3rd Quarter, pp. 121-138.
 Sheridan, T. B., 1986, "Human Supervisory Control of Robot Systems," *Proceedings, International Conference on Robotics and Automation*, San Francisco, Calif., Apr., pp. 808-812.
 Stewart, D., 1965-1966, "A Platform with Six Degrees of Freedom," *Proceedings of the Institute of Mechanical Engineers*, Vol. 180, Part I, No. 15, pp. 371-386.
 U.S. Department of Commerce, 1987, International Trade Administration, "1987 U.S. Industrial Outlook."

APPENDIX I

Robot Crane Stiffness Matrix for No Suspended Weight

In (McCallion et al., 1979) the stiffness matrix of a robot wrist device with kinematic properties similar to the robot crane suspension mechanism proposed here was derived. In that work it was assumed that the wrist displacements are

small, that the wrist weight can be ignored ($W = 0$), and that $b = 2a$ (see Fig. 3).

Here the generalized stiffness matrix K_0 of the same mechanism for any values of a or b , with no suspended weight ($W = 0$) and small displacements is derived. This stiffness is produced by the elastic deformation of the lower platform suspension system of the six wireropes each one acting as a linear spring of constant stiffness k .

For a small rigid body displacement $\delta u = [\delta u_x, \delta u_y, \delta u_z, \delta \theta, \delta \psi, \delta \phi]^T$ of the lower triangle platform from its resting steady state position, where δu is expressed with respect to the (x, y, z) Cartesian coordinate frame embedded in the lower triangle (see Fig. 4), the wireropes length change is given by

$$\delta l = \Delta \delta u \quad (20)$$

where $\delta l = [\delta l_1, \delta l_2, \delta l_3, \delta l_4, \delta l_5, \delta l_6]^T$ and Δ is the compatibility matrix.

It can easily be shown that for small changes in the wire-rope length

$$\delta l_n = [L_n(L_n' - L_n)]/l_n, \text{ for } n = 1 \text{ to } 6 \quad (21)$$

where L_n and L_n' represent the n th wire-rope vector before and after the rigid body movement, respectively, and l_n represents the length of the n th wire-rope before movement. In this case $l_n = l_0$.

For small angular displacements $\delta \theta, \delta \psi, \delta \phi$, the rotational transformation matrix Q given by equation (5) can be written as

$$Q = \begin{bmatrix} 1 & -\delta \phi & \delta \psi \\ \delta \phi & 1 & -\delta \theta \\ -\delta \psi & \delta \theta & 1 \end{bmatrix} \quad (22)$$

Then, substituting in equation (7) gives

$$l_i' = \Delta - D' = (-b - 2a\sqrt{3}/3\delta\phi - \delta u_x, -b\sqrt{3}/3 + 2a\sqrt{3}/3 - \delta u_y, -h + 2a\sqrt{3}/3\delta\theta - \delta u_z) \quad (23)$$

l_0 and h are the resting steady-state position wire-rope length and the height of the lower platform from the overhead carriage, respectively. $2a$ and $2b$ are the lengths of the sides of the two triangles (see Fig. 3).

Since

$$l_i = \Delta - D = (-b, (2a - b)\sqrt{3}/3, -h), \quad (24)$$

substituting in equation (21) gives

$$\delta l_i = \{b\delta u_x + (b - 2a)\sqrt{3}/3\delta u_y + h\delta u_z - 2ah\sqrt{3}/3\delta\theta + 2ab\sqrt{3}/3\delta\phi\} \quad (25)$$

The same sequence of operations can be repeated to determine $\delta l_2, \delta l_3, \delta l_4, \delta l_5, \delta l_6$, in terms of δu and the kinematic parameters of the six wires suspension mechanism. Then the compatibility matrix is found to be

$$\Delta = \{l/l_0\} \begin{bmatrix} b & (b-2a)\sqrt{3}/3 \\ -b & (b-2a)\sqrt{3}/3 \\ (a-b) & (b+a)\sqrt{3}/3 \\ a & (a-2b)\sqrt{3}/3 \\ -a & (a-2b)\sqrt{3}/3 \\ (b-a) & (a+b)\sqrt{3}/3 \\ h & -2ah\sqrt{3}/3 & 0 & 2ab\sqrt{3}/3 \\ h & -2ah\sqrt{3}/3 & 0 & -2ab\sqrt{3}/3 \\ h & ah\sqrt{3}/3 & -ah & 2ab\sqrt{3}/3 \\ h & ah\sqrt{3}/3 & -ah & -2ab\sqrt{3}/3 \\ h & ah\sqrt{3}/3 & ah & 2ab\sqrt{3}/3 \\ h & ah\sqrt{3}/3 & ah & -2ab\sqrt{3}/3 \end{bmatrix} \quad (26)$$

Using the virtual work principle, it is possible to prove (Asada et al., 1986) that the stiffness matrix is given by

$$K_0 = A' k A \quad (27)$$

where k is a diagonal stiffness matrix whose elements are the stiffnesses of the individual wireropes, which in this case are all equal to k .

Substituting from equation (26) into (27) gives

$$K_0 = \begin{bmatrix} K_1' & 0 & 0 & 0 & -K_2' & 0 \\ 0 & K_1' & 0 & K_2' & 0 & 0 \\ 0 & 0 & K_3' & 0 & 0 & 0 \\ 0 & K_2' & 0 & K_4' & 0 & 0 \\ -K_2' & 0 & 0 & 0 & K_4' & 0 \\ 0 & 0 & 0 & 0 & 0 & K_5' \end{bmatrix} \quad (28)$$

where

$$K_1' = 4k(a^2 + b^2 - ab) \frac{1}{l_0^2}$$

$$K_2' = 2ka(2a - b)h \frac{1}{l_0^2}$$

$$K_3' = 6kh^2 \frac{1}{l_0^2}$$

$$K_4' = 4ka^2h^2 \frac{1}{l_0^2}$$

$$K_5' = 8ka^2b^2 \frac{1}{l_0^2}$$

$$l_0 = \sqrt{h^2 + 4(b^2 + a^2 - ab)}/3$$

Comparing equations (28) and (18) reveals that $K_1', K_2', K_3', K_4', K_5'$, are equal to the first term of K_1, K_2, K_3, K_4, K_5 , respectively, if $l_n = l_0$ and $h_n = h$.

APPENDIX II

Robot Crane Stiffness Matrix due to the Weight Pendulum Effect

In this section the stiffness matrix K_w due to the pendulum effect of the suspended weight W is derived.

Single External Force in the Horizontal Direction. Assume that the six wire-rope crane suspension mechanism is modelled by a single wire-rope of length h_w with a payload of total weight W . Let an external horizontal direction force f_x along the x -axis be applied to the center of gravity of the payload giving rise to a small displacement δu_x as it is shown in Fig. 14.

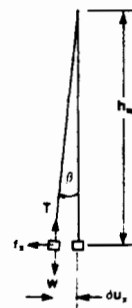


Fig. 14 Pendulum model schematic

If β is the angular displacement of the wire rope from its vertical resting position and T its new tension force (see Fig. 14), then the force balance equations give

$$W = T \cos \beta \quad \text{and} \quad f_x = T \sin \beta \quad (29)$$

Solving equations (29) for f_x , assuming a small angular displacement β and that the wire rope elongation can be neglected gives

$$f_x = \frac{W}{h_w} \delta u_x \quad (30)$$

Similarly, for an external horizontal force f_y along the y -axis applied to the center of gravity of the payload and giving rise to a displacement δu_y ,

$$f_y = \frac{W}{h_w} \delta u_y \quad (31)$$

Single External Force in the Vertical Direction. Let T be the tension force and l the length of the six wire ropes at the resting steady-state position when a weight W is suspended. Then the force balance gives

$$W = 6T \frac{h_w}{l} \quad (32)$$

Let a vertical direction force f_z along the z -axis, which is much smaller than W , be applied to the center of gravity of the lower platform resulting in a small displacement δu_z . Again assuming that the wire rope elongation can be neglected the force balance gives

$$W + f_z = 6T \frac{h_w + \delta u_z}{l} \quad (33)$$

Solving equations (32) and (33) for f_z gives

$$f_z = \frac{W}{h_w} \delta u_z \quad (34)$$

Single External Moment in the Horizontal Direction. Figure 15 shows the lower triangular platform and the no. 2 wire rope at the resting steady-state position and total suspended weight W . The vertical direction component T_{z2} along the z -axis, of the wire rope tension force T is given by

$$T_{z2} = T \frac{h_w}{l} \quad (35)$$

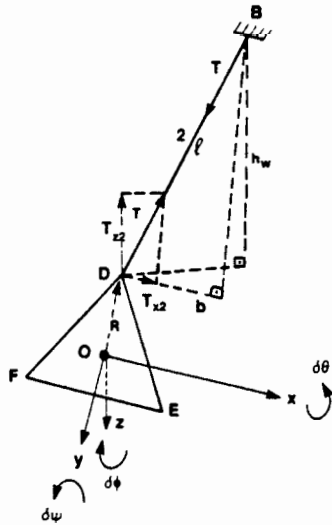


Fig. 15 Lower platform and wire rope

Let an external moment M_x along the x -axis direction be applied to the lower platform resulting in a small angular displacement $\delta\theta$ (see Fig. 15). Again assuming that the wire rope elongation can be neglected the change in the wire rope tension component T_{z2} is given by

$$\delta T_{z2} = T \frac{\delta h_{w2}}{l} \quad (36)$$

where δh_{w2} is the amount of vertical displacement by which the point D rises due to the platform rotation given by

$$\delta h_{w2} = -R\delta\theta = -2\frac{\sqrt{3}}{3}a\delta\theta \quad (37)$$

Substituting from equations (37) and (32) into equation (36) gives

$$\delta T_{z2} = -\frac{\sqrt{3}}{3^2} \frac{aW}{h_w} \delta\theta \quad (38)$$

Similarly, it can be shown that

$$\begin{aligned} \delta T_{z2} &= \delta T_{z1}, \delta T_{z3} = \delta T_{z4} = \delta T_{z5} \\ &= \delta T_{z6} = \frac{\sqrt{3}}{3} \frac{aW}{6h_w} \delta\theta \end{aligned} \quad (39)$$

Taking the moments of the wire rope tension forces with respect to the x -axis passing through center of gravity of the overhead carriage platform gives

$$\begin{aligned} M_x &= 2\frac{\sqrt{3}}{3}b(\delta T_{z4} + \delta T_{z5}) \\ &\quad - \frac{\sqrt{3}}{3}b(\delta T_{z1} + \delta T_{z2} + \delta T_{z3} + \delta T_{z6}) \end{aligned} \quad (40)$$

Substituting from equations (38) and (39) gives

$$M_x = ab \frac{W}{3h_w} \delta\theta \quad (41)$$

The same procedure can be followed in the case of an external moment M_y along the y -axis direction of the lower platform resulting in a small angular displacement $\delta\psi$ to obtain

$$\delta T_{z3} = -\delta T_{z6} = \frac{aW}{6h_w} \delta\psi \quad (42)$$

$$M_y = b(\delta T_{z3} - \delta T_{z6}) = ab \frac{W}{3h_w} \delta\psi \quad (43)$$

In this case, only wire ropes nos. 3 and 6 contribute to the moment expression.

Single External Moment in the Vertical Direction. Let an external moment M_z along the vertical z -axis direction be applied to the lower platform resulting in a small angular displacement $\delta\phi$ (see Fig. 15). Again, assuming that the wire rope elongation can be neglected, the change in the wire rope horizontal tension force component T_{x2} is given by

$$\delta T_{x2} = -\frac{W}{6h_w} R\delta\phi = -\frac{\sqrt{3}}{3^2} \frac{aW}{h_w} \delta\phi \quad (44)$$

Due to symmetry

$$M_z = -6\frac{\sqrt{3}}{3}b\delta T_{x2} = ab \frac{2W}{3h_w} \delta\phi \quad (45)$$

Combining equations (30), (31), (34), (41), (43), (45), the stiffness matrix of the suspension mechanism due to the weight pendulum effect \underline{K}_w becomes

$$\underline{K}_w = \begin{bmatrix} K_1'' & 0 & 0 & 0 & 0 & 0 \\ 0 & K_1'' & 0 & 0 & 0 & 0 \\ 0 & 0 & K_3'' & 0 & 0 & 0 \\ 0 & 0 & 0 & K_4'' & 0 & 0 \\ 0 & 0 & 0 & 0 & K_4'' & 0 \\ 0 & 0 & 0 & 0 & 0 & K_5'' \end{bmatrix} \quad (46)$$

where

$$K_1'' = K_3'' = \frac{W'}{h_w}$$

$$K_4'' = ab \frac{W'}{3h_w}$$

$$K_5'' = ab \frac{2W'}{3h_w}$$

Comparing equations (46) and (18) reveals that K_1'' , K_3'' , K_4'' , K_5'' , are equal to the second term of K_1 , K_3 , K_4 , K_5 , respectively. Thus, the suspension mechanism linearized model stiffness matrix \underline{K} can be expressed as the superposition of the no load model stiffness matrix \underline{K}_0 and the pendulum effect model stiffness matrix \underline{K}_w .